April, 2011

Thermodynamics of the antiferromagnetic Heisenberg model on the checkerboard lattice

Ehsan Khatami, *Georgetown University*
Maros Rigol, *Georgetown University*

Thermodynamics of the antiferromagnetic Heisenberg model on the checkerboard lattice

Ehsan Khatami and Marcos Rigol
Department of Physics, Georgetown University, Washington DC, 20057, USA
(Received 23 September 2010; revised manuscript received 15 December 2010; published 21 April 2011)

Employing numerical linked-cluster expansions (NLCEs) along with exact diagonalizations of finite clusters with periodic boundary condition, we study the energy, specific heat, entropy, and various susceptibilities of the antiferromagnetic Heisenberg model on the checkerboard lattice. NLCEs, combined with extrapolation techniques, allow us to access temperatures much lower than those accessible to exact diagonalization and other series expansions. We show that the high-temperature peak in specific heat decreases as the frustration increases, consistent with the large amount of unquenched entropy in the region around maximum classical frustration, where the nearest-neighbor and next-nearest-neighbor exchange interactions (J and J', respectively) have the same strength, and with the formation of a second peak at lower temperatures. The staggered susceptibility shows a change of character when J' increases beyond $0.75J$, implying the disappearance of the antiferromagnetic order at low temperatures. For $J' = 4J$, in the limit of weakly coupled crossed chains, we find large susceptibilities for stripe and Néel order with $\mathbf{Q} = (\pi/2, \pi/2)$ at intermediate temperatures. Other magnetic and bond orderings, such as a plaquette valence-bond solid and a crossed-dimer order suggested by previous studies, are also investigated.

DOI: 10.1103/PhysRevB.83.134431 PACS number(s): 75.10.Jm, 75.40.Mg, 05.70.−a, 75.40.Cx

I. INTRODUCTION

The checkerboard lattice is a unique two-dimensional (2D) system of great current interest. The next-nearest-neighbor (NNN) interactions, which are present on every other plaquette in a checkerboard pattern, not only can impose frustration and drive the system to exotic ground states but also provide a great tool for numerical and analytical investigators to study the evolution of physical properties in transitions between different geometries. For instance, in the limit of weak NNN interactions, it is expected that the physics associated with the simple square lattice is dominant. In the antiferromagnetic Heisenberg (AFH) model, this means a tendency toward long-range Néel ordering at temperatures smaller than the characteristic energy scale set by the nearest-neighbor (NN) magnetic exchange interaction, J. Whereas a ferromagnetic (negative) NNN exchange interaction, J', favors this Néel ordering, an antiferromagnetic (positive) one introduces frustration and, thus, new types of ordering such as a valence-bond solid emerge. In the fully frustrated region where $J \sim J' > 0$, the lattice is a projection of the three-dimensional corner-sharing tetrahedrons (pyrochlore lattice) onto a 2D lattice. The other interesting limit is $J' \gg J$, where the 2D lattice is practically reduced to weakly coupled crossed chains, and physical properties are dominated by those of the one-dimensional (1D) system. Moreover, by eliminating certain bonds, one can even turn the focus from the square basis of the underlying lattice to a triangular one that can capture the geometry of the Kagomé lattice.

The problem of the frustrated AFH model on the checkerboard lattice has its roots in early studies on its three-dimensional counterpart, the pyrochlore lattice. The latter system was originally studied by Harris *et al.*[1] using quantum field theory. They ruled out the possibility of a phase with long-range spin correlations but found strong correlation between NN spins, suggesting a dimerized ground state. A few years later, using perturbative expansions and exact diagonalization, Canals and Lacroix[2] concluded that the ground state is a spin-liquid with correlations that decay exponentially by distance. Around the same time, another study by Isoda and Mori,[3] in which a bond-operator approach was used, suggested a resonant-valence-bond-like plaquette phase.

So far, the magnetic properties of the checkerboard lattice have been the focus of many theoretical studies,[4–19] with compelling evidence that the ground state for $J' = J$ (the planar pyrochlore) is a plaquette valence-bond solid (P-VBS) with long-range quadrumer order.[4,6–10,12] This was shown by means of strong-coupling expansion,[4,6] exact diagonalization,[7] as well as mean field theory[10] and a quadrumer boson approximation.[9]

In the limit of $J' \ll J$, the existence of the long-range Néel order has also been established.[7,13–15] Semiclassical approaches, such as the linear spin-wave,[14,15] and numerical results[7,13] predict the stability of antiferromagnetic (AF) long-range order for $J'/J \lesssim 0.75$. However, this number is different in other studies that associate the instability of the P-VBS phase, as J' is reduced, with the transition to the Néel state (5/8 in Ref. 9, and 0.88–0.94 in Ref. 6).

The situation in the limit of weakly coupled crossed chains ($J' \gg J$) is less clear. There are at least two proposals for the ground state in this region of the parameter space; the first is the 2D spin-liquid ground state (sliding Luttinger liquid) characterized by the absence of long-range order and by elementary excitations being massless deconfined spinons.[5] This idea is supported by an exact diagonalization study of Sindzingre *et al.*,[13] which suggests a range of $J/J' = 0$–0.8 for the 1D behavior. However, their calculations suffer from strong finite-size effects even with 36 sites due to the quasi-1D nature of the problem. The second is the crossed-dimer (CD) phase suggested by Starykh *et al.*[9] They argued that, in the CD phase, staggered dimer correlations, which have a power-law decay with distance in a perfect 1D system, are stabilized when a weak interchain interaction (J) is present. As depicted in Fig. 1(e), in this phase, the "strong" (positive) dimers from perpendicular chains meet at the same crossed plaquette. This scenario is in agreement with the results of Arlego *et al.*,[16] who examined this idea by means of series expansion in terms of J and J' connecting the blocks of crossed dimers. Including

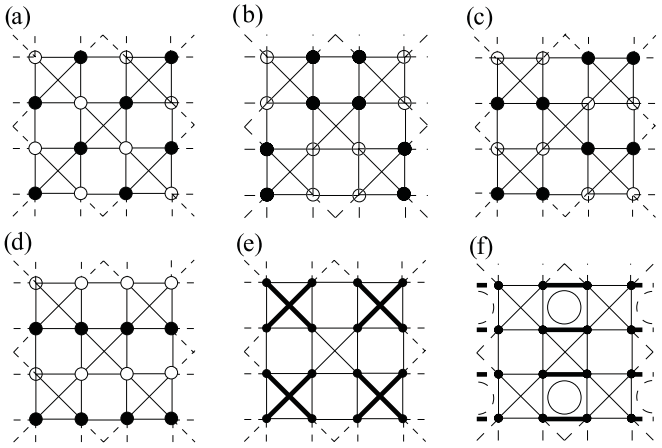

FIG. 1. Various ordered phases on the checkerboard lattice explored in this work: Néel order with (a) $\mathbf{Q} = (\pi,\pi)$, (b) $\mathbf{Q} = (\pi/2,\pi/2)$ (Néel*), (c) $\mathbf{Q} = (\pi/2,\pi)$, and (d) $\mathbf{Q} = (0,\pi)$ (stripe). Open (solid) circles denote down-spins (up-spins); (e) crossed-dimer order where thick (thin) diagonal lines represent strong (weak) bonds; and (f) P-VBS phase with strong dimer-dimer correlation between parallel bonds of uncrossed plaquettes marked by big circles.

results from other works, Starykh *et al.*[9] also mapped out the global zero-temperature phase diagram of the system with respect to the ratio of J and J' and discussed the possibility of a magnetically ordered phase being present in the transition between the CD phase and the P-VBS phase. This so-called Néel* phase is the long-range ordered phase with diverging susceptibility at $\mathbf{Q} = (\pi/2,\pi/2)$ [see Fig. 1(b)]. Most recently, using a two-leg ladder to construct the 2D lattice in a density matrix renormalization group study and by measuring various spin-spin correlations, Moukouri[17] confirmed most of these predictions for the phase diagram except that the magnetically ordered phase in the proximity of the CD phase has a wave vector $\mathbf{Q} = (\pi/2,\pi)$ instead of the $\mathbf{Q} = (\pi/2,\pi/2)$ proposed in Ref. 9. Sketches of the former order, along with the other orders explored here, are shown in Fig. 1.

Most of the numerical calculations for the AFH model on the checkerboard lattice have been done at zero temperature using finite clusters with periodic boundary condition. As discussed above, some of the early works[7,13,18] helped shape theories that describe ground-state properties such as the P-VBS. However, a systematic study of finite-temperature properties in the thermodynamic limit, more relevant to experiments, has been missing. Our goal in this study is to explore the thermodynamic properties of this model and address the finite-temperature behavior of the susceptibilities to the ordered phases proposed for the ground state and described above.

We employ the numerical linked-cluster expansions (NLCEs),[20,21] along with exact diagonalization of finite clusters, to calculate thermodynamic properties of the system in different regions of the parameter space. We study the change in behavior of energy, entropy, specific heat, and several susceptibilities as J and J' vary. We find that the high-temperature peak in specific heat is strongly suppressed in the case of maximum classical frustration, $J' = J$. Consistently, we see large amounts of unquenched entropy in this region, signaling the possibility of a second peak in specific heat. Our study of different susceptibilities includes the staggered susceptibility, which for $J'/J \leqslant 0.75$ continues to grow as the temperature is lowered, suggesting that the ground state is Néel ordered with $\mathbf{Q} = (\pi,\pi)$ in this region. We also study the susceptibility to the the P-VBS phase using relevant order parameters and find that it is largest for $J' \sim J$. In the limit of weakly coupled crossed chains, and down to the lowest temperatures we can access, the dominant correlations belong to the Néel* and stripe phases.

The paper is organized as follows. In Sec. II, we present the model and briefly discuss NLCEs and the extrapolation techniques, along with the clusters utilized in the exact diagonalizations. The results are presented in Sec. III, and a summary and conclusions are provided in Sec. IV.

II. MODEL AND NUMERICAL APPROACH

A. The Hamiltonian

The AFH Hamiltonian can be written as

$$H = J \sum_{\langle i,j \rangle} \mathbf{S}_i \cdot \mathbf{S}_j + J' \sum_{\langle\langle i,j \rangle\rangle} \mathbf{S}_i \cdot \mathbf{S}_j, \tag{1}$$

where $\mathbf{S}_i$ is the spin-1/2 vector at site i, and $\langle i,j \rangle$ denotes bonds between NN sites i and j; $\langle\langle i,j \rangle\rangle$ denotes bonds between NNN sites i and j on every other square in a checkerboard pattern.

B. Numerical linked-cluster expansions

NLCEs are linked-cluster expansion methods which allow one to calculate the partition function and other observables, per lattice site, in the thermodynamic limit at finite temperatures. The information for these quantities at a given temperature is built up by calculating contributions from all the clusters, up to a certain size, that can be embedded in the infinite lattice. Unlike high-temperature expansions (HTEs), each cluster is solved exactly using full diagonalization algorithms. Hence, NLCEs have a region of convergence which extends beyond that of HTEs. Depending on the type of ordering that occurs in the system at low temperatures, NLCEs can remain converged down to surprisingly low temperatures. Examples of these can be seen in the case of geometrically frustrated magnetic systems such as the Kagomé lattice, where there is no long-range magnetic ordering.[20–22] As in other series expansion approaches, we use extrapolation techniques to perform the summation of existing orders to further decrease the temperature of convergence, and we often gain access to regions where most of the interesting phenomena take place. More details about these extrapolations can be found in the following subsection and references therein.

Depending on the symmetry of the lattice and properties of the model, the generation of clusters in NLCEs can be done using different building blocks. These include the usual bond expansion, site expansion, triangle or square expansions, etc.[21] In this paper, we focus on the square expansion, which offers a particularly convenient approach in constructing the checkerboard lattice, i.e., by tiling it with crossed squares. In this picture, the first order in the expansion has a single crossed square, the second order has two crossed squares, and so on.

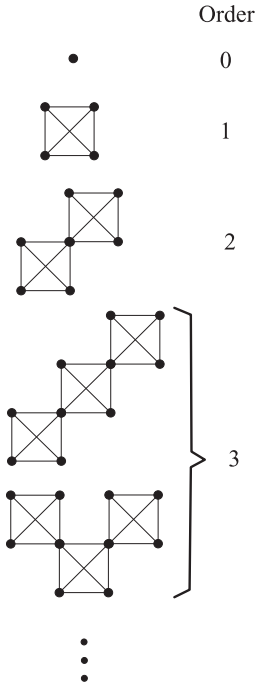

FIG. 2. Clusters generated in the first four orders of NLCE with a square building block on the checkerboard lattice.

The first four orders, including the zeroth order with a single site, are shown in Fig. 2.

In the square expansion, the maximum number of sites of a cluster in the nth order is $3n + 1$. Also, the number of topologically distinct clusters increases exponentially as the order increases. The number of clusters of each size, which need to be considered up to sixth order, is shown in Table I. Note that, out of 31 clusters in the sixth order, 23 have 19 sites, 7 have 18 sites, and 1 has 17 sites. Since the clusters have open boundaries, no translational symmetries can be used to block-diagonalize the Hamiltonian matrix. This restricts the calculations to sixth or fewer orders, where, by using the conservation of the total spin in the z direction, we have to diagonalize matrices with linear size as large as $\binom{19}{9} = 92\,378$. This is nearly impossible using serial LAPACK subroutines on single-processor machines given memory restrictions and the time needed for such huge diagonalizations. Therefore, most of the calculations have been performed on parallel computers using SCALAPACK routines.

TABLE I. Size and number of topologically distinct clusters up to the sixth order of the square expansion.

Order	Number of sites	Number of clusters
0	1	1
1	4	1
2	7	1
3	10	2
4	12	1
4	13	4
5	15	1
5	16	10
6	17	1
6	18	7
6	19	23

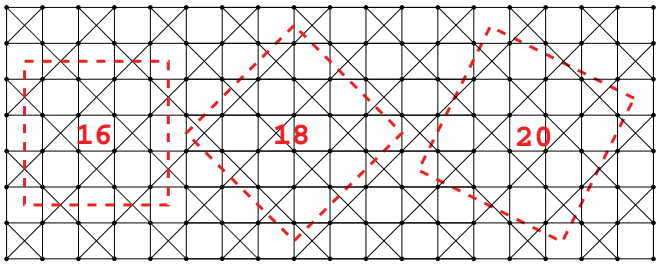

FIG. 3. (Color online) Periodic clusters on the checkerboard lattice used in our finite-size exact-diagonalization calculations. The number inside each cluster represents its size.

Where possible, we compare results from NLCEs to those from exact diagonalization of finite clusters with periodic boundary conditions (ED) to build intuition about the finite-size effects that might have influenced results of previous studies. These clusters, with 16, 18, and 20 sites, are shown in Fig. 3. We use translational symmetries that are allowed on the checkerboard lattice and are not prohibited by the symmetries of the order parameters in the broken symmetry cases. The largest matrix we had to diagonalize in this case was for the 20-site cluster, which had a linear dimension of 36 956.

C. Extrapolations

Measurements from all the clusters of every NLCE order are grouped together before summing different orders either regularly (bare sums) or by using Euler[23] or Wynn[24] sequence extrapolation algorithms. (For a detailed description of these algorithms see Ref. 21.) In the Euler sum, one can choose to have bare sums up to a particular order before using the Euler algorithm for the remaining orders. Here, we apply the Euler sum to the last four, three, two, and one terms. We find that the one with three Euler sums is generally the best (more physically sensible). In the Wynn sum, we can have one or two cycles of improvement, each eliminating two terms, leaving us with four and two terms, respectively, out of the initial six. Because of the small number of terms in the Wynn sum, we find that using only one cycle yields a more reliable outcome. Hence, unless otherwise mentioned, we show results throughout this paper for the Wynn sum with one cycle and for the Euler sum for three terms.

The behavior of these extrapolations can be seen in Fig. 4, where we show, as an example, the energy per site (E) versus temperature for $J = 0.50$ and $J' = 1.00$. We also include the bare sums up to the fifth and sixth orders, which start diverging around $T = 0.4J'$. As expected, the results from the Euler and Wynn sums show a less divergent behavior and extend the region of convergence to lower temperatures. To have a rough estimate for energy at temperatures not accessible by bare NLCE sums, we take the average of the last two terms in the Euler and Wynn sums (solid line). All these four extrapolations lie in the shaded (yellow) region which can serve as the "confidence limit." We refer to this region around the average as the error bar, although it by no means represents statistical error bars. Below the temperature where bare NLCE

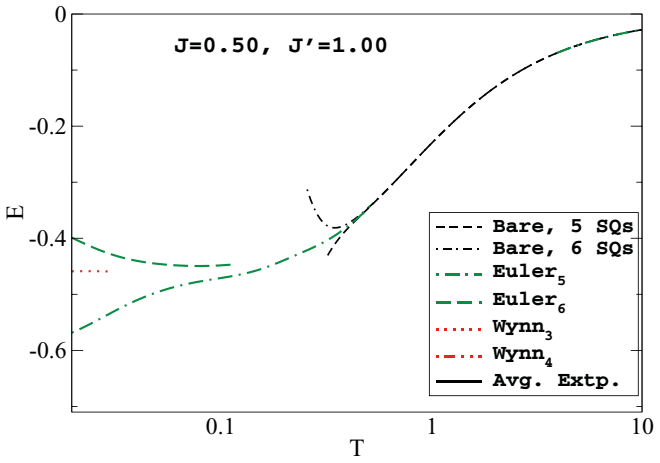

FIG. 4. (Color online) Energy per site vs temperature for the AFH model on the checkerboard lattice with NN and NNN exchange interactions $J = 0.50$ and $J' = 1.00$, respectively. The thin dashed and dot-dashed lines represent the bare NLCE sums up to the fifth and sixth orders of the square expansion. The solid line shows the average of the last two terms in the Euler and Wynn extrapolations with the shaded (yellow) area representing the "confidence limit" where all the extrapolations lie. The unit of energy is J'.

sums diverge, the extrapolations' average is not guaranteed to be the exact result in the thermodynamic limit. However, along with the error bars, it serves as an estimate of the desired quantity.

III. RESULTS AND DISCUSSIONS

Here we study thermodynamic properties such as total energy, entropy, specific heat, and several magnetic susceptibilities for a range of parameters, sweeping different regions of the phase diagram, from the simple square lattice without the NNN interaction to near the 1D limit where NNN interactions dominate. For most of these quantities, we show results for $J' = 0.00$, 0.25, 0.50, 0.75, and 1.00 when $J = 1.00$ and $J = 0.75$, 0.50, and 0.25 when $J' = 1.00$. The unit of energy is set to $\max(J, J')$.

A. Energy, entropy, specific heat, and bulk susceptibility

The specific heat per site (C) provides valuable information about the state of the system in different regions of the parameter space. In Fig. 5, we show this quantity after extrapolations of NLCE results for a range of values of J'/J. For comparison, results from ED with 18 and 20 sites are also shown. The highest peak appears for the simple square lattice with no frustration [see Fig. 5(a)]. One can see that the bare NLCE results for fifth and sixth orders (dashed and dot-dashed lines, respectively) start deviating at $T \sim 0.8$, where the antiferromagnetic correlations presumably exceed the linear size of our biggest clusters. However, the average extrapolation captures a peak around $T = 0.6$. More interesting, both ED curves depart from the exact curve at a temperature greater than J and show almost no improvement by increasing the cluster size from 16 to 20, with a position of the peak which

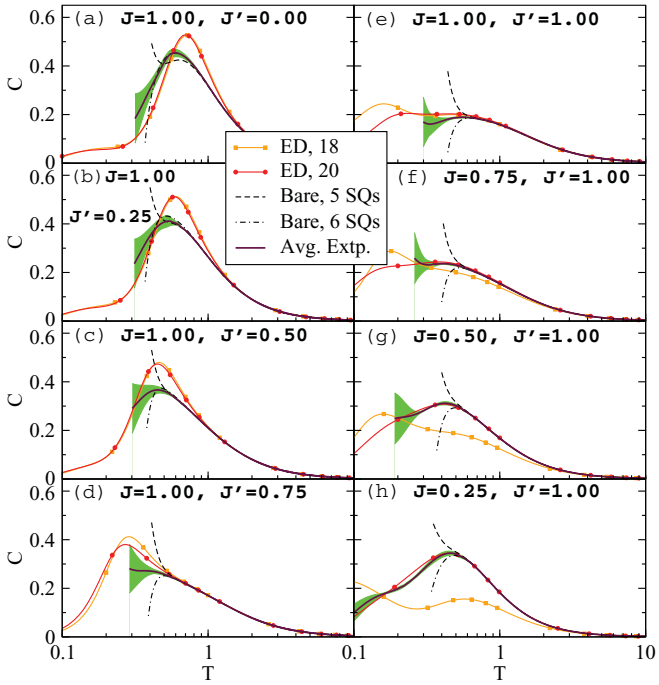

FIG. 5. (Color online) Specific heat vs temperature for various J and J': (a–d) $J' < J$ and (e–h) $J' \geqslant J$. For comparison, results from ED with 18 and 20 sites are shown. The first peak is captured for all cases after extrapolation. The NLCE results are cut off roughly where the error bars exceed 0.1. The unit of energy is set to $\max(J, J')$.

is at slightly higher temperature. (The 16-site results are not shown.)

As J'/J increases to 0.5 [Figs. 5(b) and 5(c)], the peak in specific heat broadens, its maximum value decreases, and the temperature at which the latter is reached also decreases. Due to the increase in frustration, the AF correlations are suppressed and ED more accurately predicts the location of the peak while still overestimating its value. For the same reason, the convergence in the bare NLCE sums is extended from $T \sim 0.8$ for $J' = 0.0$ to $T \sim 0.5$ for $J' = 0.5$. Further increasing J' to 0.75 [Fig. 5(d)] changes these features qualitatively by strongly suppressing the peak. In ED, the peak is pushed to lower temperatures ($T \sim 0.3$) and the agreement with exact NLCE results can be seen down to lower temperature ($T \sim 0.5$), where the bare NLCE sums also diverge. These observations are consistent with results from previous studies that find a transition at zero temperature from the magnetically ordered Néel phase to a disordered phase for $J' \gtrsim 0.75J$.[14,15]

As expected, the minimum peak value is seen for the fully frustrated case of Fig. 5(e), where $J' = J$ [see also Figs. 6(e) and 6(f)]. Although ED is in good agreement with NLCEs for $T > 0.5$, one can see significant finite-size effects at lower temperatures between the 18- and 20-site clusters. The integral of C/T for the temperature range shown for the average extrapolation curve only recovers about half of the entropy at infinite temperature, whereas 88% is recovered for the case of Fig. 5(a) with no frustration. At $T = 0.3$, the specific heat shows the tendency to develop a second peak. This tendency can be seen in both the NLCE and the ED results and, along with the fact that there is a huge amount of unquenched entropy

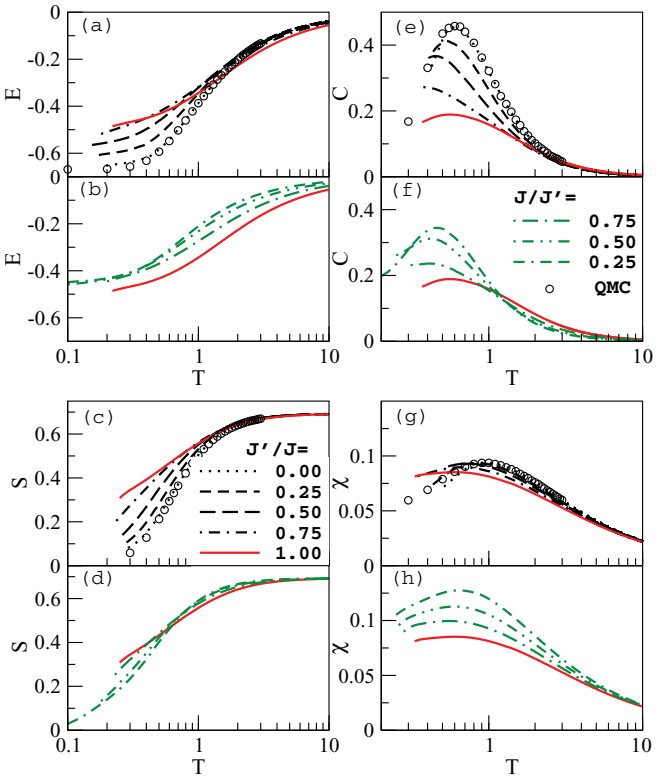

FIG. 6. (Color online) The evolution of (a, b) energy, (c, d) entropy, (e, f) specific heat, and (g, h) bulk susceptibility per site as J and J' change. These results are taken from the average extrapolations of NLCE and are cut off where the error bars reach 10% or less. Circles in (a), (e), and (g) are the data from a large-scale quantum Monte Carlo (QMC) simulation for $J' = 0$ (Ref. 25). Circles in (c) are the result of a direct integration of C/T over temperature using the QMC results in (e), plus an additive constant to recover the infinite-temperature entropy, i.e., to account for the missing low-temperature tail of the specific heat. The statistical error bars for the QMC are smaller than the symbols and are not shown.

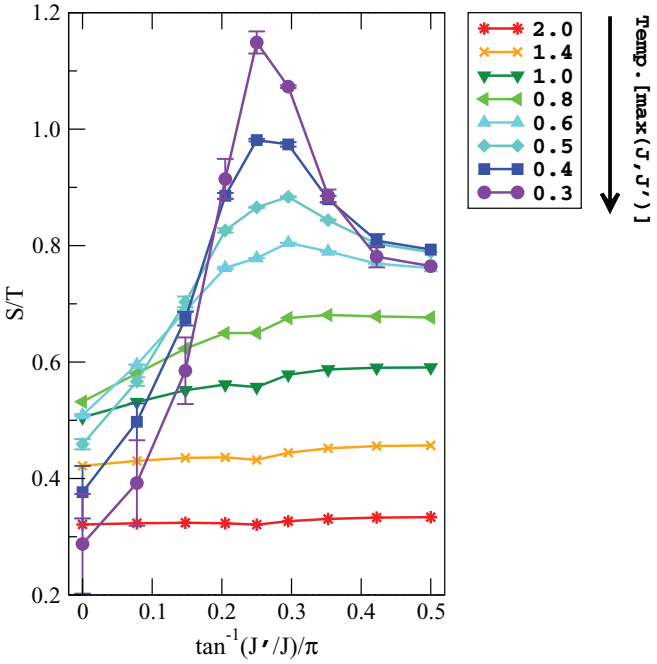

FIG. 7. (Color online) Entropy divided by temperature as a function of frustration angle, $\tan^{-1}(J'/J)$. A peak in entropy develops at $J = J'$ as temperature is lowered below 0.5. The values and the error bars are taken from the average extrapolation of NLCE results.

already at $T \sim 0.3$ [see Figs. 6(c) and 6(d)], strongly suggests that there is a second peak in specific heat at $T < 0.3$.

As the value of J/J' decreases from 1, the peak in specific heat, shown in Figs. 5(f)–5(h), increases again and the 2D system starts to behave more and more like a 1D chain. This can be inferred from the dramatic finite-size effects in ED. While the 20-site cluster can recover the NLCE results with relatively good accuracy, the results for the 18-site cluster start deviating from NLCEs at temperatures as high as 2.0. This can be understood from the fact that in the limit of decoupled crossed chains, $J = 0$, the 18-site cluster contains six decoupled periodic chains, each consisting of only three sites, whereas the 20-site cluster contains two 10-site decoupled chains. Note that not only are the 1D decoupled chains in the 18-site cluster significantly smaller, but they also contain an odd number of chain sites, i.e., AF correlations are geometrically frustrated, and this strongly affects the results. Due to the quantum fluctuations, any long-range order is suppressed near the 1D limit, and so the extrapolations capture the specific heat with much smaller error bars for $J'/J = 4$ as seen in Fig. 5(h).

In Fig. 6, we show the evolution of energy, entropy (S), specific heat, and uniform susceptibility (χ) per site as the value of J'/J changes. One can see that the energy per site at temperatures below 0.2 increases monotonically as J' increases and, as expected from the results in Fig. 5, the low-temperature entropy [Figs. 6(c) and 6(d)] is maximal in the case of $J' = J$. The previously discussed decrease of the maximum value of the specific heat by increasing J' to J, followed by an increase for larger values of $J' > J$, is more clearly seen in Figs. 6(e) and 6(f). Finally, Figs. 6(g) and 6(h) show that the uniform susceptibility remains small in all regions with a downturn below $T = 1.0$. We have also included results from a large-scale stochastic series expansion QMC simulation (circles) with up to 256×256 spins for the unfrustrated case of $J' = 0$ (Ref. 25) using directed loop updates.[26,27] This is the only case that we consider where the low-temperature QMC calculation is not limited by the sign problem.

To better compare the behavior of the entropy in different regions, in Fig. 7 we show the entropy divided by temperature as a function of the frustration angle defined as $\phi = \tan^{-1}(J'/J)$. By lowering the temperature below 0.5, the entropy develops a peak at $J' = J$, which persists down to the lowest accessible temperature (with reasonable error bars for all angles). In the square lattice limit $\phi = 0$, the specific heat and, therefore, the entropy are known to be quadratic in T at low temperatures. As can be seen in this figure, our results are consistent with this finding for T 0.5. However, by increasing J'/J to 1.0, this behavior changes completely and entropy decreases even more slowly than T. On the other hand, close to the 1D limit $\phi > 0.4\pi$, the entropy has a linear region around $T = 0.5$ below which it decreases faster than T, similar to the weakly frustrated regions with small ϕ.

B. Order parameter susceptibilities

Other than the uniform susceptibility, which can be measured directly from the fluctuations of the total spin in the z direction, other susceptibilities per site are calculated using their definition as the second derivative of the free energy with respect to the field that couples to the corresponding order parameter ($\mathcal{O}$):

$$\chi^{\mathcal{O}} = \frac{T}{N}\frac{\partial^2 \ln Z}{\partial h^2}\bigg|_{h=0}, \tag{2}$$

where N is the number of sites, Z is the partition function, and h is the field that couples to the order parameter in the new Hamiltonian, $\hat{H}' = \hat{H} - h\hat{\mathcal{O}}$. For example, we consider the following order parameter for Néel orderings with different wave vectors:

$$\hat{\mathcal{O}}_{\text{Néel}} = \sum_{\mathbf{R}} e^{i\mathbf{Q}\cdot\mathbf{R}} S^z(\mathbf{R}), \tag{3}$$

where $\mathbf{Q} = (q_x, q_y)$, $\mathbf{R}$ runs over a Bravais lattice with the basis $\mathbf{a} = (\frac{\pi}{q_x}, 0)$ and $\mathbf{b} = (0, \frac{\pi}{q_y})$, and $S^z(\mathbf{R})$ is the total spin in the z direction in the corresponding unit cell.

We find that the staggered susceptibility, $\chi^{\text{stg}}[\mathbf{Q} = (\pi,\pi)]$, at low temperatures changes character when J'/J is increased from 0.75 to 1.00. As can be seen in Fig. 8, χ^{stg} continues to grow by decreasing temperature in the weakly frustrated region and as long as $J'/J \lesssim 0.75$, but it shows a downturn at low T for $J'/J \gtrsim 1.00$. This is more clearly seen in the inset of Fig. 8, where we have plotted the inverse of the staggered susceptibility versus temperature, and is consistent with previous findings[7,13–15] which suggest that, in the latter region, the system no longer exhibits long-range Néel order. Note that the calculation of the staggered susceptibility for the unfrustrated case of $J' = 0$ is one of the worst-case scenarios for NLCEs because the antiferromagnetic correlation length

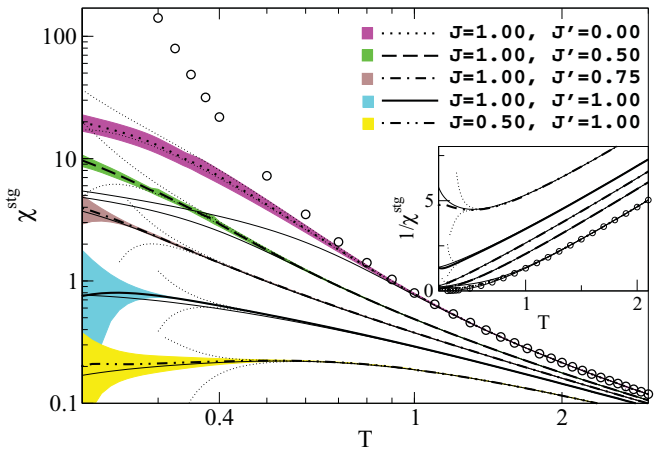

FIG. 8. (Color online) Log-log plot of extrapolated NLCE results for staggered susceptibility vs temperature. By introducing J', the staggered susceptibility is suppressed. When $J = J'$, χ^{stg} is more than one order of magnitude smaller than in the case of $J' = 0$. In the Euler extrapolation, only the last two terms have been used. The thin dotted lines are bare NLCE sums up to fifth and sixth orders. The thin solid lines represent the results from ED with 20 sites, and circles represent large-scale QMC results for $J' = 0$ (Ref. 25). The statistical error bars for the QMC results are smaller than the symbols and are not shown.

grows exponentially by decreasing the temperature. This can be realized by comparing the NLCE curve to the finite-size-converged (thermodynamic limit) QMC results (circles). Similar to the specific heat, the NLCE results start deviating from the exact solution around $T = 0.8$. Nevertheless, NLCEs provides a far better estimate for this quantity at low temperatures than ED.

According to the Mermin-Wagner theorem,[28] the Heisenberg model with finite-range exchange interactions in two dimensions cannot undergo a phase transition to a long-range ordered state at finite temperature by breaking a continuous symmetry. However, in light of the recent analytical and numerical predictions for the ground-state phases of this system, we calculate the finite-temperature susceptibilities associated with various order parameters to study their behavior as the temperature is lowered. These susceptibilities are shown in Figs. 9 to 12 in a low-temperature window for the relevant values of J and J'.

In Fig. 9, we show the susceptibility to a plaquette order which is expected to be large in the P-VBS phase around $J' = J$. Fouet *et al.*[7] argued that the ground-state wave function in this phase is the symmetric combination of the pairs of singlets on parallel bonds of the uncrossed plaquettes. Based on that, we consider the following four-spin order parameter:

$$\hat{\mathcal{O}}_4 = 32 \sum_{\bigcirc} \mathbf{S}_{l1}\cdot\mathbf{S}_{l2}\,\mathbf{S}_{l3}\cdot\mathbf{S}_{l4}, \tag{4}$$

where l is the position of every other uncrossed square, marked by a circle in Fig. 1(f). The spin numbers around each of these squares are such that 1 and 2 (and therefore 3 and 4) are nearest neighbors. Since this kind of order involves uncrossed squares, NLCEs in crossed squares are not suited to measure the corresponding susceptibility, and so we have obtained results only from ED. They show that this susceptibility is largest in the region around the maximum classical frustration. However, significant finite-size effects are seen, especially for the $J' = J$ case. In this region, the results for the 16-site cluster deviate from those for the 20-site cluster when $T < 1.0$, with the susceptibility being roughly a factor of 2 larger at $T \sim 0.1$ for the 16-site cluster. Interestingly, for the 20-site cluster, the susceptibility shows a significant decrease by further decreasing temperature below $T = 0.07J$. Note that most of the thermodynamic quantities, such as the specific heat and other susceptibilities calculated using ED (even with 20 sites), deviate from their exact NLCE counterparts (bare sums) starting from temperatures as high as 0.5 in this parameter region. So, the peak feature is expected to be a consequence of the finite-size nature of the calculations. We tested a more sophisticated order parameter suggested in Ref. 7 to better capture the P-VBS phase, namely, the four-spin cyclic permutation operator $(P_4 + P_4^{-1})$,[29] and found the same qualitative results as for $\hat{\mathcal{O}}_4$ after rescaling.

Alternatively, one can define a simple two-spin order parameter as the sum of strong NN bonds around every other empty plaquette and weak NN bonds elsewhere to describe this phase:

$$\hat{\mathcal{O}}_2 = \sum_{\square} (-1)^{l_x}(\mathbf{S}_{l1}\cdot\mathbf{S}_{l2} + \mathbf{S}_{l2}\cdot\mathbf{S}_{l3} + \mathbf{S}_{l3}\cdot\mathbf{S}_{l4} + \mathbf{S}_{l4}\cdot\mathbf{S}_{l1}), \tag{5}$$

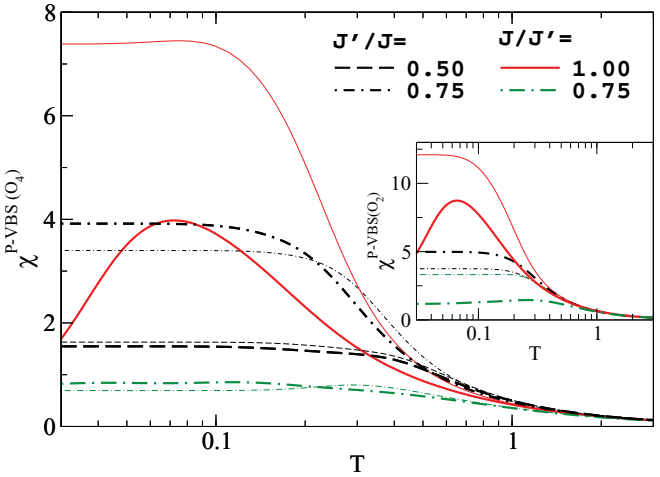

FIG. 9. (Color online) ED results for the susceptibility to the P-VBS order [see Eq. (4)] per site vs temperature. Thick (thin) lines are results for the 20-site (16-site) cluster. The order is depicted in Fig. 1(f). The inset shows the susceptibility to the two-spin version of the plaquette order parameter as presented in Eq. (5).

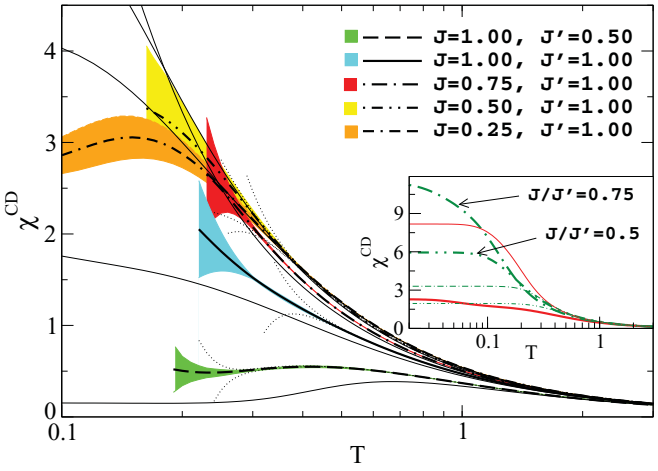

FIG. 10. (Color online) Susceptibility to the crossed-dimer order [see Eq. (6) and Fig. 1(e)] per site vs temperature. Thin dotted lines are the last two orders of bare NLCE sums, and thin solid lines are the ED results with 20 sites. In the Euler extrapolation, only the last two terms have been used. In the inset, lines are as in Fig. 9 with thick (thin) lines representing ED results for the 20-site (16-site) cluster.

where l is the position of each empty square (□) in units of the NN lattice spacing and we have numbered the spins in each square clockwise, starting from the bottom left corner. The resulting susceptibilities for three values of J'/J around the fully frustrated region are plotted in the inset of Fig. 9 and show similar trends as their four-spin counterparts.

By decreasing J/J' to 0.5, we find that the low-temperature susceptibility to the CD order is enhanced (Fig. 10). To calculate this susceptibility, we consider the following order parameter:

$$\hat{\mathcal{O}}_{\rm CD} = 2 \sum_{\boxtimes} (-1)^{l_x} (\mathbf{S}_{l1} \cdot \mathbf{S}_{l3} + \mathbf{S}_{l2} \cdot \mathbf{S}_{l4}), \qquad (6)$$

where l is the position of each crossed square (⊠) and spin numbering is the same as in Eq. (5) so that $\mathbf{S}_1$ and $\mathbf{S}_3$ (or $\mathbf{S}_2$ and $\mathbf{S}_4$) are at the two ends of diagonal bonds. Although this susceptibility is significantly larger for $J'/J > 1$, the extrapolated values for $J'/J = 4$ exhibit a downturn at finite temperature. The results from ED with 20 sites overestimate the NLCE results at low T for $J' > J$. However, we see significant finite-size effects between the 16- and 20-site clusters, shown in the inset of Fig. 10. We have checked the susceptibility to a closely related order parameter in which there is one strong diagonal bond on every crossed plaquette [specifically, Eq. (6) with a minus sign between the two terms] and found a behavior qualitatively similar to the CD susceptibility but with smaller values (not shown). Since the CD phase was predicted to exist for $J' \gg J$,[9] an interesting question posed by these results is whether the peak feature will eventually disappear for smaller values of J/J' and one would find a susceptibility that always increases with decreasing temperature. In this scenario, the relevant temperature at which the CD phase becomes dominant is $\mathcal{O}(J^2/J')$[9], which is beyond the convergence region of our current NLCE calculations.

We find that for large values of $J'/J > 2$ (weakly coupled crossed chains) there are two magnetic orderings that are dominant at the lowest temperatures we can study. They are (i) the so-called Néel* order and (ii) stripes along the horizontal (or vertical) directions (Figs. 11 and 12). The corresponding order parameters are defined in Eq. (3) with $\mathbf{Q} = (\pi/2,\pi/2)$ and $\mathbf{Q} = (0,\pi)$ and are depicted in Figs. 1(b) and 1(d), respectively. The former has been proposed theoretically as the candidate for this region.[9] An intriguing observation is that the values for these two susceptibilities are hardly distinguishable, especially when $J' > J$. To illustrate the latter, we plot the NLCE results for the Néel* susceptibility against the stripe susceptibility in Fig. 12 (circles). One can see that the relative difference is negligible for all values of J'/J shown.

These results are consistent with what one would expect at intermediate temperatures in the limit of $J' \gg J$, because both orders are compatible with the antiferromagnetic correlations that develop along the diagonal chains. We note that for the ED with the 16-site cluster, using adjacency matrices, one can show that the modified Hamiltonians, $\hat{H}'$, are identical for the two order parameters. It would have been interesting to compare ED results for both orders with larger system sizes; however, given the unit cell size for each order (eight sites for the Néel* and four sites for the stripe) and our computational limitations with increasing system sizes, those results are only available for the stripe order and are shown in Fig. 12. Resolving which order becomes dominant at lower temperatures will require the study of larger cluster sizes, both in NLCEs and in ED. It is worth mentioning that, based on numerical calculations, the stripe order was suggested to be the one relevant to the ground state of the $J_1 - J_2$ model when $J_2 \gtrsim 0.6 J_1$.[17]

We have explored another magnetic ordering suggested by Mokouri[17] to be dominant in the limit $J' \gg J$. It has a wave vector of $\mathbf{Q} = (\pi/2,\pi)$ and a unit cell of eight sites. Because of the breaking of certain symmetries of the lattice, the

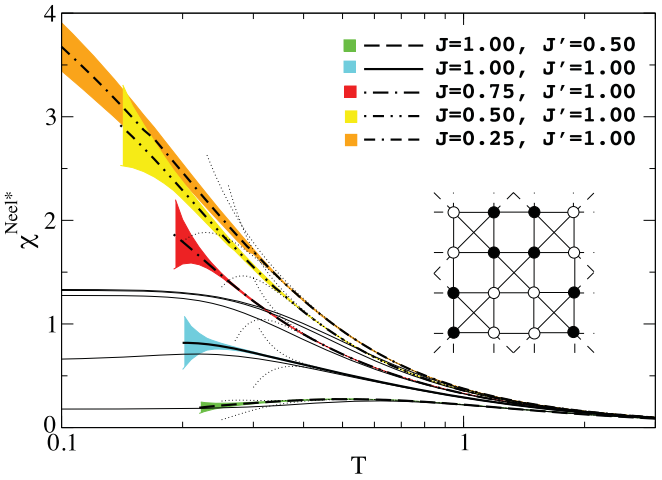

FIG. 11. (Color online) Néel* susceptibility [$\mathbf{Q} = (\pi/2,\pi/2)$] per site vs temperature for a range of ratios of J and J'. The inset shows the corresponding magnetic order where the open (solid) circles represent down-spins (up-spins). Thin dotted lines are the last two orders of bare NLCE sums, and thin solid lines are the ED results with 16 sites.

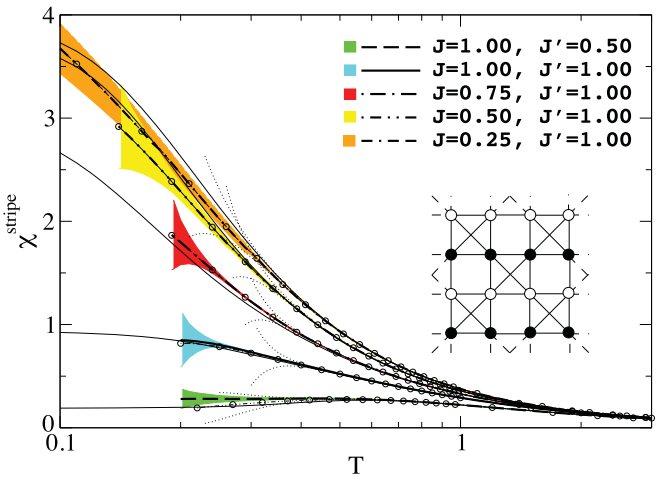

FIG. 12. (Color online) Susceptibility to the stripe order [$\mathbf{Q} = (0,\pi)$] per site vs temperature. The inset shows the corresponding magnetic order where the open (solid) circles represent down-spins (up-spins). Thin dotted lines are the last two orders of bare NLCE sums, and thin solid lines are the ED results with 20 sites. Circles are NLCE results for the Néel* order (Fig. 11).

NLCE calculations for this case become much more expensive because one has to compute the physical properties of each cluster at different orientations and locations on the lattice to properly deal with the broken symmetry. (This applies to the previously mentioned orders as well, but, due to the presence of other symmetries, computations are less costly in those cases.) Thus, we only present results from ED with 16 sites for this type of order. As shown in Fig. 13, not only is this susceptibility smaller close to the 1D limit, but the maximum value, which belongs to the case of $J' = J$, is also much smaller than the maximum value seen for other orders with 16 sites (see, e.g., Fig. 11). Therefore, a transition to this phase seems unlikely in any of the parameter regions. The fact that this type of order is not favored close to the 1D limit is not surprising since, unlike in the Néel* or stripe ordered phases, spins on diagonal chains are not antiferromagnetically aligned.

IV. SUMMARY

We have calculated the thermodynamic properties of the AFH model on the checkerboard lattice using NLCEs and ED and studied their behavior as the system crosses over from a simple square lattice ($J' = 0$) to the maximally frustrated planar pyrochlore lattice ($J' = J$) to the limit of one-dimensional crossed chains ($J' \gg J$).

We found that the peak value in the specific heat is suppressed as the frustration increases (by increasing J'/J from 0 to 1), with strong indications that there is a second peak in the specific heat for $J' \sim J$. In the same region, finite-size effects in ED are minimal for temperatures above the convergence limit of NLCE. In contrast, close to the 1D limit, ED results can vary significantly from one cluster to the other, depending on the size of periodic 1D chains that exist inside each 2D cluster. Consistent with the reduced specific heat, entropy is maximal when $J' = J$ at low temperatures with a decrease that is slower than T.

We calculated the susceptibilities to several magnetic and bond orderings to explore the tendencies of the system toward different phases as the temperature is decreased. By studying the staggered susceptibility, we found that the tendency toward Néel ordering with $\mathbf{Q} = (\pi,\pi)$ decreases appreciably when $J'/J \gtrsim 0.75$. By increasing the NNN interaction, antiferromagnetic correlations along the diagonal chains become important and other types of order emerge. To investigate this, we examined the susceptibility to the P-VBS order using ED and found that it is largest for $J' \sim J$. We also found large finite-size effects between 16- and 20-site clusters for $J' = J$.

We further explored the susceptibility of the CD order, which is larger for $J' > J$ but, according to the extrapolated NLCE results and for the values of J and J' considered

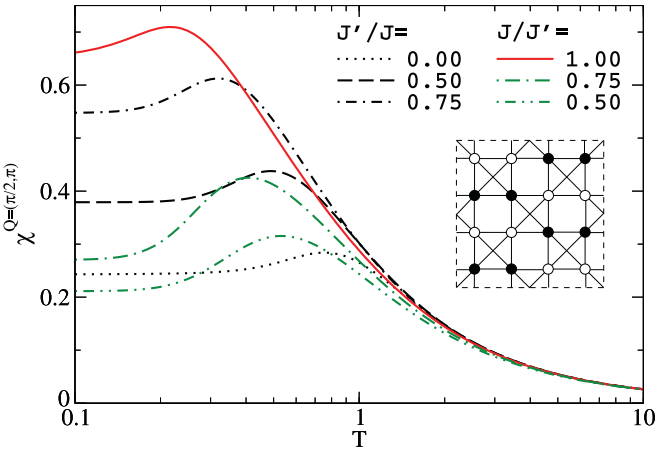

FIG. 13. (Color online) Susceptibility to the Néel order with $\mathbf{Q} = (\pi/2,\pi)$ per site, calculated using ED with 16 sites, vs temperature. The inset shows the corresponding order where open (solid) circles represent down-spins (up-spins).

here, does not dominate at the intermediate temperatures accessible within our NLCEs. Finite-size effects between the 16- and 20-site clusters were found to be significant in the ED calculations for $J' \geqslant J$. When $J' > 2J$, i.e., for weakly coupled crossed chains, we found fast increasing susceptibilities at intermediate temperatures to Néel* order with $\mathbf{Q} = (\pi/2,\pi/2)$, suggested by analytical results, and stripe order with $\mathbf{Q} = (0,\pi)$. Both of these orders are favored in this region due to the antiferromagnetically aligned spins along the chains.

ACKNOWLEDGMENTS

This research was supported by the National Science Foundation (NSF) under Grant No. OCI-0904597 and enabled by the allocation of advanced computing resources, supported by the NSF. Part of the computations were performed on Ranger and Lonestar at the Texas Advanced Computing Center under Account No. TG-DMR100026. We thank Stefan Wessel for providing us with the QMC results and for helpful discussions. We are grateful to Rajiv R. P. Singh and Oleg Starykh for careful reading of the manuscript and their useful comments.

[1] A. B. Harris, A. J. Berlinsky, and C. Bruder, J. Appl. Phys. **69**, 5200 (1991).
[2] B. Canals and C. Lacroix, Phys. Rev. Lett. **80**, 2933 (1998).
[3] M. Isoda and S. Mori, J. Phys. Soc. Jpn. **67**, 4022 (1998).
[4] W. Brenig and A. Honecker, Phys. Rev. B **65**, 140407 (2002).
[5] O. A. Starykh, R. R. P. Singh, and G. C. Levine, Phys. Rev. Lett. **88**, 167203 (2002).
[6] W. Brenig and M. Grzeschik, Phys. Rev. B **69**, 064420 (2004).
[7] J.-B. Fouet, M. Mambrini, P. Sindzingre, and C. Lhuillier, Phys. Rev. B **67**, 054411 (2003).
[8] O. Tchernyshyov, O. A. Starykh, R. Moessner, and A. G. Abanov, Phys. Rev. B **68**, 144422 (2003).
[9] O. A. Starykh, A. Furusaki, and L. Balents, Phys. Rev. B **72**, 094416 (2005).
[10] R. Moessner, O. Tchernyshyov, and S. Sondhi, J. Stat. Phys. **116**, 755 (2004).
[11] E. Berg, E. Altman, and A. Auerbach, Phys. Rev. Lett. **90**, 147204 (2003).
[12] J.-S. Bernier, C.-H. Chung, Y. B. Kim, and S. Sachdev, Phys. Rev. B **69**, 214427 (2004).
[13] P. Sindzingre, J.-B. Fouet, and C. Lhuillier, Phys. Rev. B **66**, 174424 (2002).
[14] R. R. P. Singh, O. A. Starykh, and P. J. Freitas, J. Appl. Phys. **83**, 7387 (1998).
[15] B. Canals, Phys. Rev. B **65**, 184408 (2002).
[16] M. Arlego and W. Brenig, Phys. Rev. B **75**, 024409 (2007).
[17] S. Moukouri, Phys. Rev. B **77**, 052408 (2008).
[18] S. E. Palmer and J. T. Chalker, Phys. Rev. B **64**, 094412 (2001).
[19] E. H. Lieb and P. Schupp, Phys. Rev. Lett. **83**, 5362 (1999).
[20] M. Rigol, T. Bryant, and R. R. P. Singh, Phys. Rev. Lett. **97**, 187202 (2006).
[21] M. Rigol, T. Bryant, and R. R. P. Singh, Phys. Rev. E **75**, 061118 (2007).
[22] M. Rigol and R. R. P. Singh, Phys. Rev. Lett. **98**, 207204 (2007); Phys. Rev. B **76**, 184403 (2007).
[23] H. W. Press, B. P. Flannery, S. A. Teukolsky, and W. T. Vetterling, *Numerical Recipes in Fortran* (Cambridge University, Cambridge, UK, 1999).
[24] A. J. Guttmann, *Phase Transitions and Critical Phenomena* (Academic, London, 1989), Vol. 13.
[25] S. Wessel (private communication).
[26] A. W. Sandvik, Phys. Rev. B **59**, R14157 (1999).
[27] F. Alet, S. Wessel, and M. Troyer, Phys. Rev. E **71**, 036706 (2005).
[28] N. D. Mermin and H. Wagner, Phys. Rev. Lett. **17**, 1133 (1966).
[29] D. J. Thouless, Proc. Phys. Soc. Lond. **86**, 893 (1965).